FLIGHT DYNAMIC SIMULATION OF A FLAPLESS FLIGHT CONTROL UAV

A.Buonanno*, M.V.Cook**

Dynamics, Simulation and Control Group,
School of Engineering, Cranfield University,
Cranfield, Bedfordshire, MK43 0AL, UK

Keywords: *Flapless, flight, control, circulation, UAV*

Abstract

This paper describes the flight dynamics contribution to a research programme in which the objective is to design, develop and fly a UAV utilising flapless flight control. A circulation control actuator concept has been tested and a Simulink model is being developed for incorporation into the aircraft simulation. Results show that bi-directional proportional control of the air vehicle is feasible.

Notation

b	Wing span
b_j	Span of the slot
c	Mean aerodynamic chord
C_L	Lift coefficient
C_M	Pitching moment coefficient
C_μ	Momentum coefficient
h_j	Height of the slot
M	Mach number
$\dot{m}_j$	Mass flow rate of jet thorough slot
P	Pressure
q_∞	Dynamic pressure
R	Gas constant
S	Wing reference area
T	Temperature
V_j	Average speed of jet at slot
V_∞	Free stream velocity
α	Angle of attack
δ	Control angle
γ	Ratio of specific heat
ζ	Damping
ω	Frequency

1 Introduction

The FLAVIIR project is a five year research programme looking at technologies for future unmanned air vehicles (UAV) funded jointly by BAE Systems and the Engineering and Physical Sciences Research Council (EPSRC) in the UK. Managed jointly by BAE Systems and Cranfield University, the project includes nine additional collaborating university partners. The research programme covers all essential aspects of aeronautical technologies integration for the next generation of advanced UAV concepts. The focus for the research is the "Grand Challenge" proposed by BAE Systems:

"To develop technologies for maintenance free, low cost UAV without conventional control surfaces and without performance penalty over conventional craft"

The principal goal of this ambitious programme of research is to design, build and fly a small, but representative, UAV embodying the integrated technologies developed in the various research studies comprising the project. In particular, it is intended to demonstrate the feasibility of total flight control utilizing flapless technologies. In the context of the project, flapless flight control is interpreted to mean circulation control on the wing by means of trailing edge blowing and thrust vectoring the exhaust from the small propulsive gas turbine engine.

In support of the project a programme of flight dynamics research is underway in which the main objective is to provide modelling,

simulation and stability and control analysis to the collaborating partners. This paper describes some of that research, in particular the application and modelling of circulation control technology for the purpose of representative flight simulation.

1.1 Circulation Control

The characteristic of a wall jet remaining attached to a curved surface is well known and dates back to 1800 when Young first described the phenomenon and which was later named the *Coanda effect* after Henri Coanda in 1910. The Circulation Control (CC) Wing concept is based on the application of the Coanda effect and involves converting the airfoil trailing edge into an enlarged rounded surface to which a jet of air adheres when blown tangentially from the upper surface. Although the idea is certainly not new, it was not seriously investigated until the early 1960s by Dunham [1], and later by Kind [2].

Dunham focused on application of CC to a circular cylinder and his work describes a method for representing the lift of circulation control airfoils with external flow. The work of Kind is related to that of Dunham and represents a considerable extension of that method. He developed a calculation method to determine the blowing coefficient C_μ for a given lift coefficient C_L. However, determining the performance of CC airfoils using analytical methods has proven to be extremely difficult due to the viscous flow region that must be modelled. There are strong interactions between the jet region and the overall flow due to circulation coupling, and an accurate analysis of the flow field requires a procedure that accounts for the highly coupled viscous and inviscid regions. This could not be done by simple potential analysis until the 1980s when many numerical studies were conducted and which examined the application of the Navier-Stokes equations to predict the aerodynamic characteristic of CC airfoils. A summary of these studies is given by Liu [3]. However, a completely satisfactory design code is still not available. In the 1970s Experiments by Englar [4], Abramson [5] and others examined the

effect of a wide range of parameters on circulation control airfoils. This research tended to concentrate on experimental studies of two dimensional aerofoil sections. Application of the circulation control concept to a three dimensional aircraft wing was first demonstrated at West Virginia University in April 1974 on a CC Technology Demonstrator STOL[6] aircraft, and five years later in 1979 on a modified Navy Grumman A-6A[7] aircraft.

Recently, experimental evaluations were also conducted on the High Speed Civil Transport (HSCT) aircraft [8], [9]. A circulation control airfoil with dual radius trailing edge section, initially applied to a Boeing 737-200, was integrated into a full size HSCT configuration. These studies found that the advanced high-lift devices produced a large increase in lift with a significant drag reduction, and confirmed the effectiveness of combined pneumatic high-lift devices and conventional flap control surfaces on the HSCT aircraft. Of particular note, the application of circulation control was shown to reduce the take-off field length by as much as 31% from the reference point.

More recently, research focused on the performance benefits for a CC delta wing with regions of separated flow was carried out at Manchester University [10], [11]. A combined experimental and computational fluid dynamics study of the low speed aerodynamic benefit achievable through the application of circulation control to a delta wing was performed. This was perceived to offer the replacement of conventional control surfaces with the blown trailing edge of a CC wing. The initial aim of the study was to assess the feasibility of the technology for application to a tailless concept during landing to reduce the pitch attitude and, or, landing speed whilst maintaining longitudinal trim. A generic model of a delta wing planform was tested and it has been shown that circulation control can produce a significant lift increment, similar to that of a conventional high lift control surface, but with a lower pitch moment increment, resulting in improved aircraft control. All configurations tested showed lift augmentation of approximately 15

for reasonably low blowing rates. This suggests that the usable lift increment, equivalent to that achievable with existing flap systems, could be obtained with blowing coefficient of order $C_\mu \cong 0.005$. Further experimental investigations have been performed by Frith and Wood [12], [13], [14] in which the interest was focused on potential manoeuvre performance with a CC wing. An investigation into roll control was conducted at Manchester University [12] on a full span test configuration with delta wing planform, using differential upper surface blowing on either side of the full span model. The results indicated that roll control varies linearly with C_μ and the presence of the leading edge vortex augments the effect in a pro-roll capacity. This work at Manchester has led directly to the flapless flight control vehicle concept which is central to the FLAVIIR UAV research project.

2 Air Vehicle descriptions

The "Demon" air vehicle selected for the project is derived from the "Eclipse" air vehicle, a pre-existing UAV design developed at Cranfield University jointly with BAE Systems. The Eclipse air vehicle is shown in Fig. 1.

Fig. 1. The Eclipse air vehicle

Eclipse is a tailless configuration, with a cropped diamond wing planform and powered by a single AMT Olympus HP ES gas turbine engine. Table 1 shows the main geometry and mass properties of the Demon variant of the vehicle. The Eclipse air vehicle has four trailing

edge flaps either side of the centre line. Outboard and inboard flap are used symmetrically for longitudinal control and outboard aileron flaps are used differentially for lateral control. For a detailed description of the configuration refer to reference [15].
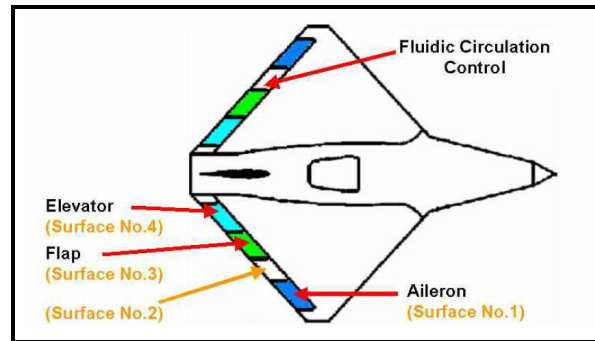

Fig. 2. The Eclipse controls configuration

Empty mass	m	42 kg
Wing area	S	2.635 m^2
Wing span	b	2.2 m
Mean chord	$\bar{c}$	0.3 m
Roll moment of inertia	I_{xx}	1.51 kgm^2
Pitch moment of inertia	I_{yy}	14.96 kgm^2
Yaw moment of inertia	I_{zz}	16.25 kgm^2
Inertia product	I_{xz}	-0.28 kgm^2

Table 1. Demon geometry and mass properties

The Demon air vehicle uses the existing Eclipse airframe modified to accommodate the new integrated technologies. Small changes to the configuration are made to permit installation of thrust vectoring and the trailing edge is modified to replace four flaps with three larger flaps either side of the centre line, of which the middle flap can be replaced with a circulation control device (see Fig 2). Since the Eclipse was marginally unstable, internal layout changes have resulted in a more forward cg to ensure a statically stable vehicle.

2.2 Demon Aerodynamic model

The aerodynamic model of the Demon was derived from Eclipse aerodynamics, with the addition of some wind tunnel test data relating to the modified flap surface distribution. The original aerodynamic data for Eclipse was developed using semi-empirical methodologies,

such as DATCOM, together with some limited basic wind tunnel data.

Linear regression analysis was applied to the Demon wind tunnel data to generate Taylor series functions that approximate the dependence of the forces and moments on angle of attack, sideslip angle and flap angle. The wind tunnel data comprised aerodynamic force and moment coefficients at various combinations of angle of attack, sideslip angle and control surface deflection. The range of variation for these parameters corresponds to the region over which the aerodynamics is nominally linear, the main implication of this simplification being that the angle of attack is limited to values below 20 degrees. Coupling terms between angle of attack and control deflection are used to account for the dependence of control effectiveness on angle of attack. Limited data and higher levels of uncertainty made it impossible to isolate Reynolds number effects for side force and moment coefficients and as a result, the values for the coefficients represent an average over the dynamic pressure range.

Additional terms were added to the Taylor series expressions in an *ad hoc* manner to account for dependence on angular rates (i.e., dynamic derivatives). Terms associated with the angle of attack and pitch rates were added to lift (CL_q, CL_α) and pitching moment (CM_q, CM_α). Terms associated with roll and yaw rates were added to side force (CY_p, CY_r), rolling moment (Cn_p, Clr) and yawing moment (Cn_p, Cn_r). The coefficients for most of these additional terms were estimated using DATCOM methods. The expression for total lift force coefficient is shown in equation (1) as an example of the Taylor series expansion.

$$C_L = C_{L_0} + C_{L_\alpha}\alpha + C_{L_\eta}\eta + C_{L_{\delta_f}}\delta_f +$$
$$+ C_{L_q}q\left(\frac{c}{2V}\right) + C_{L_{\dot{\alpha}}}\left(\frac{c}{2V}\right)\dot{\alpha} \qquad (1)$$

The expressions for drag, side force, and pitching, rolling, and yawing moments are similar in structure but differ in the particular coefficients associated with coupling.

2.3 Simulation model

A six degree of freedom simulation model has been developed, based on the Eclipse airframe, to evaluate the control and stability characteristics of the conventional flap control configuration. The simulation model is based on the aircraft equations of motion presented in Reference [16] and which were coded using Matlab/Simulink. The structure of the simulation model is depicted in the Appendix and follows standard practice.

The equations of motion are implemented in a modular format and include the 1976 standard atmosphere model. The equations represent the conventional six degree-of-freedom motion of a rigid aircraft relative to a flat, non-rotating earth.

Two major subsystems represent the vehicle dynamics in the longitudinal and lateral-directional axes respectively. The coupling between these two subsystems is due to inertial and gravitational effects. The usefulness of the simulation model was enhanced by incorporating several additional output equations, in particular air data parameters, acceleration variables and flight path variables.

As new design and aerodynamic data has become available, so the simulation model has been developed to represent the Demon configuration. This process will continue as the air vehicle design is refined.

2.4 Demon stability and control analysis

The simulation model of the Demon air vehicle was used to assess the stability and control properties of the vehicle. These analyses do not, however, constitute a validation or verification of the simulation model since there are no alternative static or dynamic data available for comparison at the present time.

First a trim map was made for the vehicle in straight level flight at several dynamic pressures. The results of two longitudinal trim studies are shown in Table 2. The velocity (30, 40 and 45 m/s) is representative of typical flight speeds of the Demon. The computed trim was obtained by using the Demon simulation model and a

constrained optimization routine to achieve level trim at a specified dynamic pressure. An alternative simplified analytical trim was determined using the method described in reference [17]. Equations (2) were solved to determine trim, angle of attack, symmetric elevon angle (η) and thrust throttle (τ) setting.

$$\frac{\tau T_X(V_\infty)}{q_\infty S} - C_X(\alpha,\eta) - \frac{W}{q_\infty S}\sin(\gamma+\alpha) = 0$$

$$C_Z(\alpha,\eta) - \frac{W}{q_\infty S}\cos(\gamma+\alpha) = 0 \qquad (2)$$

$$C_{M_{cg}}(\alpha,\eta) - \frac{\tau T_X(V_\infty)}{q_\infty S}\frac{Z_t}{\bar{c}} = 0$$

Comparison of the alternative trim analyses shows very good agreement for angle of attack, symmetric elevon deflection, and throttle setting.

Velocity (m/s)	Throttle	Angle of attack (deg)	Symmetric Elevon (deg)
Computed trim			
30	0.3	8.8	-11.6
40	0.25	5.6	-4.6
45	0.24	4.6	-2.8
Analytical Trim			
30	0.26	8	-11
40	0.23	4.4	-3.5
45	0.23	3.5	-1.3

Table 2. Analytical and simulation based longitudinal trim.

The simulation was also linearized about the above trim conditions to assess the dynamic stability characteristics of the vehicle. Table 3 shows the frequency and damping of the linearized longitudinal modes.

Velocity (m/s)	Short period		Phugoid mode	
	ζ_s	ω_s (rad/s)	ζ_p	ω_p (rad/s)
30	0.22	4	0.08	0.416
40	0.2	5.53	0.06	0.314
45	0.2	5.69	0.08	0.266

Table 3. Longitudinal stability modes.

Note that the short period mode is stable for all three velocities but lightly damped. Its frequency increases with increasing velocity but

the damping is essentially constant. The phugoid mode is adequately stable.

Table 4 shows the time constants or frequency and damping of the linearised lateral-directional modes. Note that all modes are stable, but notably, the dutch roll mode is very well damped and the spiral mode time constant is unusually short.

Velocity (m/s)	Roll mode	Spiral mode	Dutch Roll	
	T_r (s)	T_s (s)	ζ_{dr}	ω_{dr} (rad/s)
30	0.069	4.08	0.485	5.69
40	0.051	8.33	0.406	7.09
45	0.045	12.5	0.388	7.87

Table 4. Lateral-directional stability modes.

3 Circulation control actuator

A circulation control wing prototype has been demonstrated in flight by Manchester University to produce usable control forces and moments. The basic flow control arrangement requires high pressure air blown from a narrow span-wise trailing edge slot over a curved trailing edge surface as indicated in Fig. 3.
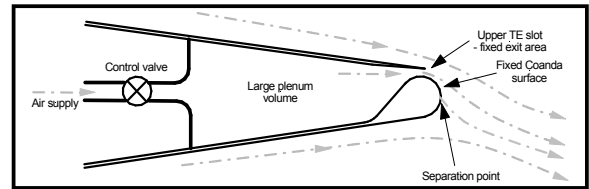

Fig. 3. Fixed trailing edge slot geometry

On-off modulation of the air supply to the slot enables unidirectional force and moment generation for control of the vehicle. Replacing conventional ailerons with spanwise pairs of slots permits differential operation sufficient for lateral control and without the adverse yaw effect of a flap surface. Modulation of the control force and moment generated by a fixed trailing edge geometry utilizing internal air flow throttling suggests a difficult engineering solution to a practical mechanism for vehicle control. Possible difficulties include increased

mechanical complexity for bi-directional control, bandwidth limitation associated with airflow throttling and the impact of back pressure variation resulting from on-off bleed air demand on a small gas turbine engine compressor.

An alternative mechanization is currently in development at Cranfield and comprises a flow control actuator fully capable of proportional bi-directional control which avoids some of the problems of fixed slot circulation control. Preliminary experiments have shown the feasibility of the device. However, at the time of writing the effectiveness of the device compared with a conventional flap control is not fully understood. Therefore, a model of the flow control device is being developed for incorporation into the Demon air vehicle simulation to facilitate performance evaluation studies.

3.1 Circulation control actuator model

The system has been modelled as shown in Fig. 4. Air is supplied continuously to the plenum chamber through a pipe. Since the total exit slot area remains constant the mass flow rate required from the system is also constant and there is no need to modulate the internal air flow trough a throttle valve. However, a control valve is required to adjust the pressure inside the plenum chamber in response to varying external conditions over the flight envelope. The moving trailing edge is actuated by means of a small model electro servo.
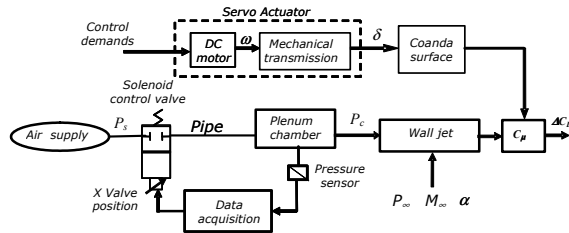

Fig. 4. Pneumatic system representation

Performance of a circulation control device is characterized as a function of slot flow momentum coefficient, C_μ, which is the momentum flux exiting from the slot

normalized by the free stream dynamic pressure and a reference area – usually the area of the wing with full span trailing edge slot:

$$C_\mu = \frac{\dot{m}_j V_j}{q_\infty S} \tag{3}$$

The ratio of the jet total pressure to free stream static pressure is specified as the blowing condition. In most instances quasi stagnation conditions are produced inside the plenum, and for a subsonic jet C_μ is,

$$C_\mu = 2\frac{h_j}{c}\frac{M^2_j}{M^2_\infty} \tag{4}$$

Where h_j/c is the ratio of the total slot height (upper+lower slot) and the mean aerodynamic chord. The local Mach number at the jet exit slot is determined from the isentropic equation expanding the plenum stagnation pressure to free stream static pressure,

$$M_j = \sqrt{\frac{2}{\gamma-1}\left(\left(\frac{P_c}{P_\infty}\right)^{\frac{\gamma-1}{\gamma}}-1\right)} \tag{5}$$

The actual ambient pressure at the slot exit is not exactly free static pressure and it is difficult to assess accurately. Thus free stream static pressure is assumed as a matter of convenience and convention. The isentropic mass flow rate is calculated using compressible flow relationships to give,

$$\frac{\dot{m}_j\sqrt{RT_c}}{A_jP_c} = \sqrt{\frac{2}{\gamma-1}\left(\frac{P_\infty}{P_c}\right)^{\frac{2}{\gamma}}\left(1-\left(\frac{P_\infty}{P_c}\right)^{\frac{\gamma-1}{\gamma}}\right)} \tag{6}$$

The mass flow requirement for specific momentum coefficients and different trailing edge slot heights are shown in Fig.5.

The effect of varying the slot height of a circulation control wing suggests a compromise between the advantages of high jet velocity or high jet momentum The smaller slots exhibit higher lift augmentation ratios as a result of their higher jet velocity for a given C_μ. Conversely higher slots heights produce

substantially higher lift coefficients, because of the higher jet momentum for a given velocity. Thus, the circulation control wing poses an optimization problem dependent upon whether the blowing air supply is mass flow or pressure ratio limited.
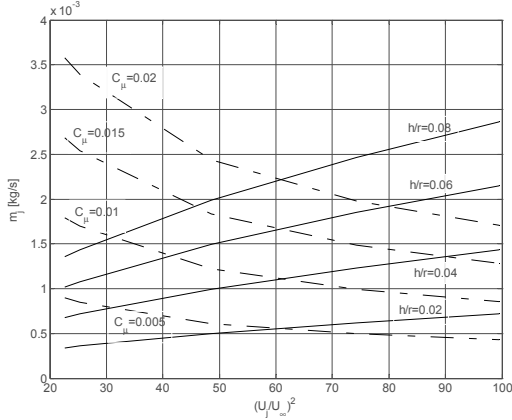

Fig. 5. Mass flow requirements for specific momentum coefficients and slot height (reference $q_\infty = 38$ Pa).

3.1.1 Pneumatic system model

The model of the pneumatic system which determines the plenum pressure follows subject to the simplifying assumptions:

1- Gas is ideal.
2- Gas density is uniform in the chamber and in the pipe.
3- Gas flow through the pipe is an isentropic process.
4- Flow in the connection port is isentropic
5- Flow leakage is negligible.
6- A quasi stagnation condition exists inside the plenum chamber
7- The ambient pressure at the slot exit is the free stream static pressure

According to assumptions (1), (2), (3)   the dynamic model of the gas in the chamber and in the pipeline is given by the following relations [18], [19]:

$$\dot{P}_c = \frac{\gamma R T_c}{V_c}(\dot{m}_c - \dot{m}_j)$$

$$\dot{P}_c = \frac{\gamma R T_p}{V_p}(\dot{m}_p - \dot{m}_c)$$

(7)

Where P_c, V_c, T_c and $\dot{m}_c$ are respectively the pressure, volume, temperature and mass flow in the plenum chamber and, P_p, V_p, T_p and $\dot{m}_p$ are the pressure, volume, temperature and mass flow respectively in the pipe. R is the ideal-gas constant and γ is the ratio of specific heats of the gaseous medium. According to assumption (3), the temperature in the chamber and in the pipe is given by the following relations:

$$T_c = T_{c0}\left(\frac{P_c}{P_{c0}}\right)^{\frac{\gamma-1}{\gamma}}$$

(8)

$$T_p = T_{p0}\left(\frac{P_p}{P_{p0}}\right)^{\frac{\gamma-1}{\gamma}}$$

Where P_0 and T_0 are the initial conditions. According to assumption (4) and (5) the flow in the valve and in the connection port are then modelled as follow:

$$\dot{m}_c = \frac{C_c A_c P_p}{\sqrt{RT_p}} f_r\left(\frac{P_c}{P_p}\right) \quad P_p \geq P_c$$

(9)

$$\dot{m}_p = \frac{C_s W_s x P_s}{\sqrt{RT_s}} f_r\left(\frac{P_p}{P_s}\right) \quad x \geq 0$$

Where A_c is the orifice area of the connection port, $W_s x$ is the geometric orifice area of the servo-valve, x is the servo-valve spool position and P_s, T_s are the pressure and the temperature respectively of the air supply. C_c and C_s are the orifice discharge coefficients. To take account of the subsonic and sonic conditions the flow function is defined as:

$$f_r = \begin{cases} \sqrt{\dfrac{2\gamma}{\gamma-1}}\sqrt{y^{\frac{2}{\gamma}} - y^{\frac{\gamma+1}{\gamma}}} & y \geq r_c \\ \sqrt{\gamma\left(\dfrac{2}{\gamma+1}\right)^{(\gamma+1)/(\gamma-1)}} & y < r_c \end{cases}$$

(10)

Where r_c is the critical pressure ratio given by $r_c = (2/\gamma+1)^{\gamma/(\gamma-1)}$.

Since the volume of the pipe is small compared to the volume of the plenum chamber, the pipe dynamic response is much faster than that of the chamber and the dynamic model of the system can be approximated by its low frequency component. Thus, a simplified dynamic model can then be defined,

$$\dot{P}_c = \frac{\gamma R T_c}{V_c}(\dot{m}_p - \dot{m}_j)$$

$$\dot{m}_c = \dot{m}_p$$

(11)

3.1.2 Servo actuator model

The position of the cylindrical bar is controlled through an electrical servo actuator. The open loop response of the system is therefore governed mainly by the transient of the actuator, since this is the slowest component in the system. Experimental measurement of the open loop response of the actuator enabled a second order model to be described with provision for non-linear delays,

$$\frac{\delta}{\delta_d} = \frac{\omega^2}{s^2 + 2\omega\varsigma + \omega^2} e^{-Ls}$$

(12)

Where δ_d the commanded deflection angle and δ is the actual deflection angle, ω is the frequency of the system ς is the damping ratio and L is the non-linear time delay. Fig.6 shows a comparison of the simulated time step response with the response of the actual servo actuator.
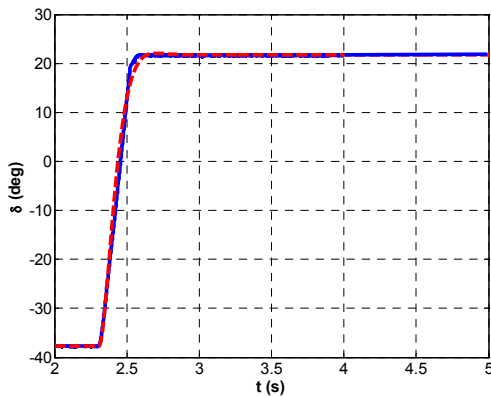

Fig.6. Comparison of test response (—) and system estimated response (---).

3.2.3 Aerodynamic model of the CC actuator

Wind tunnel experiments have been conducted on a rectangular wing [20] in which the CC actuator device was incorporated as an interchangeable replacement for an inset flap, shown in Fig.7. These experiments have shown the incremental lift to be a linear function of actuator control angle δ,
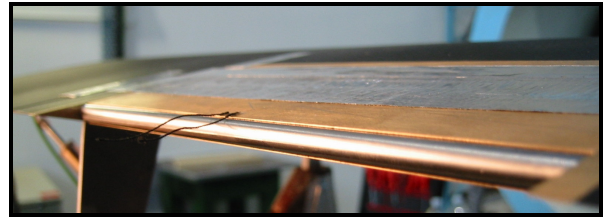
$$\frac{dC_L}{d\delta} = K$$

(13)

Fig.7.Trailing edge view of the flow control actuator

Wood [21] predicts that for low C_μ, C_L varies linearly with C_μ and the *lift augmentation* is a function of the angle of attack and Mach number. Whence,

$$\frac{dC_L}{dC_\mu} = f(\alpha, M_\infty)$$

(14)

Therefore, for a given momentum coefficient C_μ, the lift increment per unit control angle δ over the actuator control angle range can be expressed as,

$$\frac{dC_{LC_\mu}}{d\delta} = K_{C_\mu}(\alpha, M_\infty)$$

(15)

The dependency of ΔC_{LC_μ} on the value of the blowing momentum coefficient derives from the equivalent 2-D characteristic of a part span CC actuator in the trailing edge of the wing. Thus, an effective 2-D momentum coefficient can be defined based on CC actuator performance installed in a given wing planform. Let b_j be the part span trailing edge slot from equation (4) follows,

$$C_{\mu2-D} = C_{\mu3-D}\frac{b}{b_j}$$

(16)

Let S_{eff} be the fraction of wing area ahead of the part span trailing edge slot, then the full span lift increment due to the CC actuator can be expressed as,

$$\frac{dC_{L_F}}{d\delta} \approx \frac{dC_L}{d\delta}\frac{S}{S_{eff}} \qquad (17)$$

In the absence of wind tunnel tests on a 3-D Demon model with part span CC actuator, a semi-empirical ESDU method has been used to estimate the rolling moment derivative due to the operation of the CC actuator. The model assumes the Demon wing planform with inserted CC actuator spanning the same portion of the wing as the existing mechanical aileron. The method adjusts the 2-D CC actuator data for sweep, aspect ratio and partial span flap effects.

Using this procedure a rolling moment derivative for the Demon with flapless roll control was derived from the original experimental wind tunnel data for the CC actuator installed in a rectangular wing. Comparison of the lateral response to conventional aileron and to CC actuator for V_∞=40m/s and C_μ=0.01 is plotted in fig.8. Since a linear model was used for this evaluation the response shapes are similar. However, it is clear that the CC actuator is capable of similar performance to conventional ailerons.
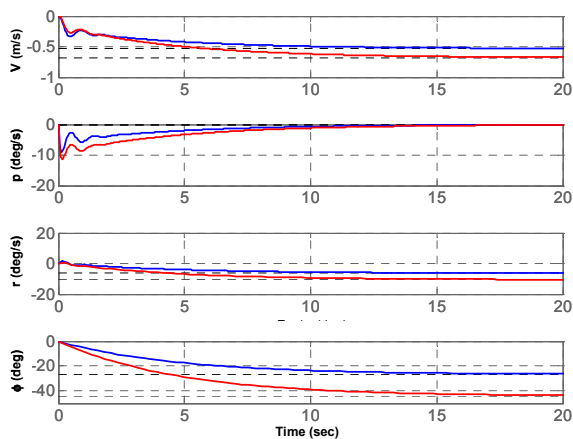

Fig. 8. Lateral response comparison for 1 deg step aileron (—) and 1 deg step CC actuator inputs (--).

Concluding remarks

A simulation model of the Demon UAV has been developed in a MATLAB/Simulink environment to provide flight dynamics support to the Flaviir research programme. A preliminary model of a flapless circulation control actuator representation has been incorporated into the simulation model and initial evaluation has shown,

- Bi-directional incremental lift generation comparable to a mechanical flap of similar trailing edge span is possible.
- Lift response to rotation of the trailing edge coanda surface through an equivalent control angle is remarkably linear.
- Roll control power equivalent to that of conventional ailerons can be achieved at practical slot blowing conditions.

Care must be exercised in the interpretation of the results as the experimental evaluations to date are for limited operating conditions.

Further research is underway to improve the overall accuracy of aerodynamic modelling and to validate the simulation model. Expansion of the CC modelling to permit full flight dynamic evaluation over the flight envelope is in progress.

References

[1] Dunham J. A theory of circulation control by slot blowing applied to a circular cylinder. *Journal of Fluid Mechanics*, Vol. 33, Part 3, pp 495-514, 1968.

[2] Kind R. J. A calculation method for circulation control by tangential blowing around a bluff trailing edge. *The Aeronautical Quarterly*, Vol. XIX.1968.

[3] Liu Y, Sankar L.N, Englar R.J and Ahuja K.K. Numerical simulations of the steady and unsteady

aerodynamic characteristics of a circulation control wing airfoil. *AIAA-2001-0704*, 2001.

[4] Englar R.J. Circulation control for high lift and drag generation on STOL aircraft. *Journal of Aircraft*, Vol. 12, No. 5, pp 457, May 1975.

[5] Abramson J. Two dimensional subsonic wind tunnel evaluation of a 20 percent thick circulation control airfoil. *DTNSRDC Report,* ASED-311, 1975.

[6] Roberts S. C. WVU circulation controlled STOL aircraft flight tests. West Virginia University, Morgantown, WV, *Aerospace TR-42*, July 1974.

[7] Pugliese A.J. Flight testing the circulation control wing. *AIAA-79-1791*, AIAA Aircraft Systems and Technology Meeting, 1978.

[8] Englar R.J, Niebur C.S, Gregory S.D. Pneumatic lift and control surface technology applied to a high speed civil transport configurations. *AIAA 97-0036,* January 1997.

[9] Mavris D.N and Kirby M.R. Take off/Landing assessment of an HSCT with pneumatic lift agumentation. *AIAA 99-0534,* 37th Aerospace Sciences Meeting and Exhibit, Reno, NV, January 11-14, 1999.

[10] Sellars, N.D, Wood N.J. and Kennaugh A. Delta wing circulation control using the coanda effect. AIAA 1st Flow Control Conference, St. Louis, June 2002.

[11] Wood N.J and Roberts L. The control of vortical lift on delta wings by tangential leading edge blowing. *AIAA-87-0158*, AIAA 25th Aerospace Sciences Meeting, Reno, Nevada, 1987.

[12] Frith S. P and Wood N.J. Circulation control high lift applications on a delta wing. CEAS Aerospace Aerodynamics Research Conference, Cambridge, June 2002.

[13] Frith S. P and Wood N.J. Investigation of dual circulation control surfaces for flight control. *AIAA 2004*-2211, 2nd AIAA Flow Control Conference 28 June, Portland Oregon, July 2004.

[14] Frith S. P and Wood N.J. Effect of trailing edge geometry on a circulation control delta wing. *AIAA 2003-3797*, 21st applied Aerodynamics Conference, Orlando, Florida, 2003.

[15] Yarf-Abbasi A and Allegri G. The Flying Demonstrator UAV configuration control document. *Flaviir project internal report*: InR151204.

[16] Stevens B.L. and Lewis F.L. *Aircraft Control and Simulation*. John Wiley and Sons, Inc., 1992.

[17] Etkin B. *Dynamics of Atmospheric Flight*. John Wiley and Sons, Inc., 1972.

[18] P. Bigras T, Wong and R. Botez**.** Pressure tracking control of a double restriction pneumatic system. IASTED *International Conference on Control and Applications*, pp.273-278, 2001.

[19] B.W. Anderson. *The Analysis and Design of Pneumatic Systems*. Wiley, New York, 1967.

[20] Buonanno A, M.V. Cook, S.D. Erbslöh. An investigation into the feasibility of a high bandwidth trailing edge circulation control actuator. *Flaviir project internal report*: AeR2004406.

[21] Wood N.J and Nielsen J. Circulation control airfoils: past present, future. *AIAA-85-0204*, AIAA 23rd Aerospace Sciences Meeting, Reno, Nevada, 1985.

Appendix

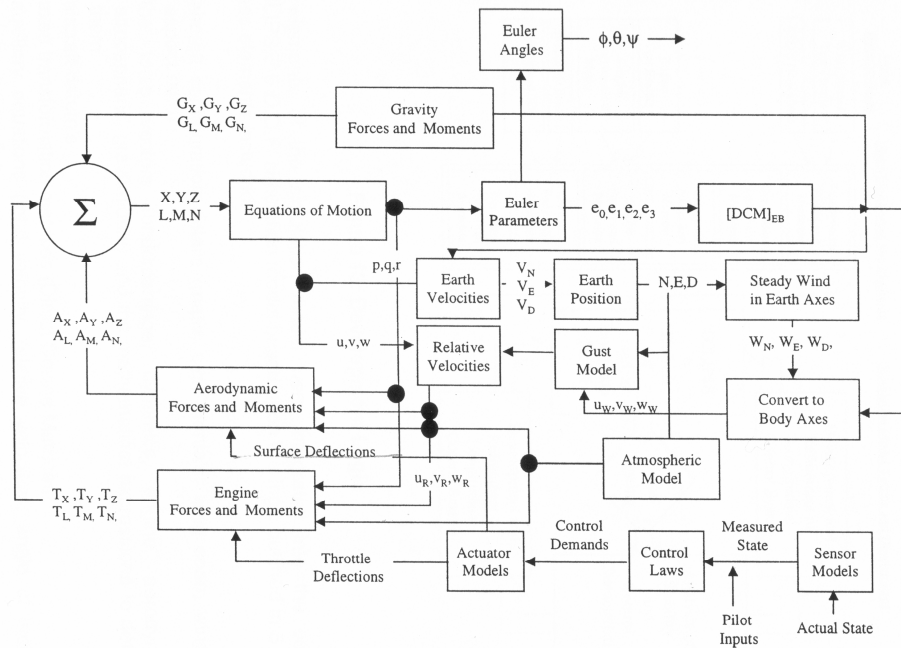The appendix contains a block diagram of the basic structure of the simulation model.

Fig. 1. Simulation block diagram